Available online at www.sciencedirect.com
SCIENCE DIRECT
Surface Science 600 (2006) 963–970
SURFACE SCIENCE
www.elsevier.com/locate/susc

Deactivation of Pd particles supported on $Nb_2O_5/Cu_3Au(100)$: SFG and TPD studies from UHV to 100 mbar

Frank Höbel, Athula Bandara, Günther Rupprechter *, Hans-Joachim Freund

Fritz-Haber-Institut der Max-Planck-Gesellschaft, Faradayweg 4–6, 14195 Berlin, Germany

Received 13 September 2005; accepted for publication 15 December 2005
Available online 19 January 2006

Abstract

Structural changes that occur on Pd–$Nb_2O_5/Cu_3Au(100)$ model catalysts upon thermal annealing were followed by sum frequency generation (SFG) and temperature-programmed desorption (TPD) using CO as probe molecule. SFG experiments were performed both under ultrahigh vacuum and mbar pressure. Heating the catalyst to temperatures above 300 K lead to an irreversible 50% decrease in the CO adsorption capacity and modified the remaining adsorption sites. Alterations of the phase between resonant and non-resonant SFG signals upon annealing indicate a change in the electronic structure of the surface, which excludes Pd sintering or migration of Nb_2O_5 over Pd particles to cause the observed effect and rather suggests the formation of "mixed Pd–NbO_x" sites. The same changes in surface properties also occur during CO hydrogenation at 1 bar and high temperature, pointing to an involvement of "mixed Pd–NbO_x" sites in catalytic reactions.

Keywords: Palladium; Niobium; Clusters; Carbon monoxide; Sum frequency generation; Thermal desorption spectroscopy; Chemisorption; Vibrations of adsorbed molecules

1. Introduction

Niobium-oxide (niobia) containing catalysts are an interesting class of materials and have recently received considerable attention. Niobia itself may be the active phase (unsupported or supported on other oxides), it may serve as support for metal nanoparticles or oxides and may also be used as promoter [1–10]. The most important applications include Fischer–Tropsch synthesis, oxidative dehydrogenation of alkanes, oxidative coupling of methane and others (see below). Studies on high-surface area niobium-oxides inherently carry a high degree of complexity because several stable structures exist (NbO, NbO_2 and Nb_2O_5) and one cannot expect that the resulting surfaces are simple truncations of bulk niobia structures. This is even more so for supported metal oxides, i.e. when two-dimensional thin niobium-oxide layers partly cover a support oxide (e.g. niobia on Al_2O_3, SiO_2, ZrO_2, TiO_2, V_2O_5, etc. [6–8]). Vice versa, Nb_2O_5 was also used as a support for overlayers of vanadium-, chromium-, rhenium-, molybdenum-, and tungsten-oxide [11–16]. These catalysts are active for selective hydrocarbon oxidation, NO_x conversion, alkene isomerization or polymerization, oxidative dehydrogenation, dehydration, partial oxidation of methanol, etc. ([12] and references therein). When Nb_2O_5 was used to support Rh and Ni particles, CO hydrogenation could be carried out with high selectivity to hydrocarbons, while Rh and Ni supported by Al_2O_3, SiO_2 or ZrO_2 yielded more methane [4,8,15–17]. As Nb_2O_5 is a reducible oxide, metal–support interaction (SMSI) was proposed as explanation [15,16]. Co particles on Nb_2O_5 also showed a high selectivity towards long chain hydrocarbons in the Fischer–Tropsch synthesis [11,12,18]. Nb_2O_5 promoted Pd/Al_2O_3, Cr_2O_3, and Mo–V catalysts

* Corresponding author. Permanent address: Institute of Materials Chemistry, Vienna University of Technology, Veterinärplatz 1, A-1210 Vienna, Austria. Fax: +43 1 25077 3890.
E-mail address: grupp@imc.tuwien.ac.at (G. Rupprechter).

0039-6028/$ - see front matter © 2006 Elsevier B.V. All rights reserved.
doi:10.1016/j.susc.2005.12.039

have been successfully tested for the oxidation of volatile organic compounds [19–23].

In order to gain a fundamental understanding of oxide surfaces, well-ordered thin film oxides, grown in ultrahigh vacuum (UHV) under well-controlled conditions, have turned out to be a successful approach ([24–29] and references therein). In contrast to many bulk oxides, thin oxide films exhibit an electric and thermal conductivity that allow the application of electron spectroscopy and temperature-programmed techniques. Furthermore, thin oxide films grown on single crystal substrates are also well-suited for laser spectroscopy [30–36]. Recently, the preparation of well-ordered thin Nb_2O_5 films was reported by Middeke et al. and Starr et al. [37] who have grown a thin niobia film on a $Cu_3Au(100)$ substrate (which was implanted with oxygen) by Nb deposition and subsequent oxidation. The structure of the Nb_2O_5 film was examined by low energy electron diffraction (LEED) and scanning tunneling microscopy (STM), its composition by angular resolved X-ray photoelectron spectroscopy (XPS) and Auger electron spectroscopy (AES). High-resolution electron energy loss spectroscopy (HREELS) and density functional theory (DFT) were applied to confirm the proposed structure. For a complete description we refer to [37], here only a brief summary is given. The Nb_2O_5 oxide film grows two-dimensionally, forming terraces ~100 nm wide, and is ~0.4 nm thick. The film consists of 2/3 ML of a Nb layer above a close packed O layer, on which Nb cations in oxidation state close to 5+ occupy hollow sites and form a $(\sqrt{3}\times\sqrt{3})R30^\circ$ structure. There is another oxygen layer on top of the Nb lattice, leading to a O–Nb–O–Cu_3Au stacking. Due to the square symmetry of the $Cu_3Au(100)$ substrate, there are two domains, rotated by 90°.

In the present study, we have utilized these Nb_2O_5 films to support Pd nanoparticles. In particular, we examine the adsorption of CO by combining temperature-programmed desorption (TPD) and sum frequency generation (SFG), the latter being applied both under UHV and pressures up to 100 mbar. The results on Pd–Nb_2O_5/$Cu_3Au(100)$ model catalysts are compared to previous studies on Pd–Al_2O_3/NiAl(110) [30,33–36]. In contrast to Pd–Al_2O_3, the Pd–Nb_2O_5 model system undergoes strong structural changes when annealed above 300 K. SFG and TDS indicated changes in the electronic structure of the surface and a strong loss of CO adsorption capacity, pointing to the formation of "mixed Pd–NbO_x" sites. The new surface structure was stable upon repeated annealing and H_2 treatments did not induce further modifications. The Pd–Nb_2O_5 model catalysts were also tested for CO hydrogenation at 1 bar using gas chromatography but no measurable activity was observed.

2. Experimental

The experiments were performed in a UHV system (base pressure $\sim 2\times10^{-10}$ mbar) consisting of two sections, (i) a preparation/characterization chamber and (ii) a high-pressure reaction cell [30,34]. The preparation chamber was equipped with an ion sputter gun for surface cleaning, LEED and AES for surface characterization, a quadrupole mass spectrometer (QMS) for TPD measurements, and metal evaporators and a quartz microbalance for deposition of Nb and Pd. The high-pressure cell had CaF_2 windows for SFG measurements and was connected to a gas chromatograph [30].

The $Cu_3Au(100)$ sample crystal was spot-welded by Ta wires to two Mo rods and could be heated resistively to 1300 K and cooled with liquid N_2 to 90 K. Clean $Cu_3Au(100)$ was obtained by cycles of Ar^+ bombardment (1 keV, 5×10^{-6} mbar for 30 min) at 500 K and annealing at 800 K for 5 min. The structure and cleanliness of the surface were examined by LEED and AES. The clean Cu_3Au surface was then sputtered at 300 K with oxygen (1 keV, 7×10^{-7} mbar O_2 for 30 min) followed by annealing at 650 K for 5 min. This treatment implants oxygen into the substrate which seems to prevent Nb/substrate alloying and also creates an oxygen reservoir facilitating the growth of Nb_2O_5 films [37–39].

Nb_2O_5 films of about 0.4 nm thickness were prepared by evaporation of ~1.5–2 Å nominal thickness of (metallic) Nb (from a Nb rod) at 300 K followed by oxidation at 773 K in 1×10^{-6} mbar oxygen for 30 min and annealing at 773 K for 30 min. The well-ordered structure of the Nb_2O_5 film was confirmed by LEED at 90 K, showing a pattern as that reported by Starr et al. [37].

Pd particles were grown on the Nb_2O_5/$Cu_3Au(100)$ substrate at 90 K via Pd deposition (by evaporation of a Pd rod) at a rate of 0.1 nm/min for 6 min, yielding, of course, a nominal Pd thickness of 0.6 nm. According to the analysis of the CO-SFG intensity (see below), the Pd particles were about 3.5 nm in size and exhibited rather rough surfaces. Apparently, the growth (island density) of Pd on Nb_2O_5 and on Al_2O_3 seems roughly comparable, at least at 90 K.

For a full description of SFG theory we refer to [30–36,40,41] and references therein. The SFG signal basically comprises two contributions, a *resonant* part arising from the vibrations of adsorbed molecules, and a *non-resonant background* arising from "off-resonance" SFG signals due to electronic transitions at the interface. As described in detail in [35], the SFG lineshape then depends on the relative magnitudes of both contributions and, in particular, on the *phase* ϕ between them. Since the *phase* ϕ is sensitive to the electronic structure of the substrate, compositional changes at the interface induce changes in ϕ and, consequently, in the SFG lineshape that can be monitored.

SFG vibrational spectroscopy was performed using a Nd:YAG laser (1064 nm, 30 mJ/pulse, 20 ps, 50 Hz) with part of the output converted to 532 nm and 355 nm by a harmonic generator. The 1064 nm and 355 nm beams were mixed in an optical parametric generator/difference frequency generator to produce tunable infrared pulses of about 150 μJ/pulse in the range of 3–6 μm, with resolution of about 5 cm^{-1}. The 532 nm light used for SFG had an energy of about 200 μJ/pulse.

The measured SFG intensities were normalized by the intensities of the incident IR and vis beams. To extract accurate values for the peak position, amplitude, full width at half maximum (FWHM) and phase ϕ the experimental data were analyzed (fitted) with a theoretical function (see [35] for details). In the SFG spectra squares represent the experimental data while solid lines are the result of the fitting procedure. All SFG spectra were measured with *p*-polarized beams. For TPD measurements, the samples were placed about 1 mm in front of a quadrupole mass spectrometer shield and were heated at a rate of 1 K/s.

3. Results and discussion

In the following, we utilize SFG and TPD to examine CO adsorption on the various surfaces in order to be able to differentiate contributions from the $Cu_3Au(100)$ substrate, the Nb_2O_5 oxide support, and the Pd–Nb_2O_5/$Cu_3Au(100)$ model catalysts.

3.1. Adsorption of CO on $Cu_3Au(100)$

Fig. 1 displays SFG and TPD spectra of CO on clean $Cu_3Au(100)$. At 100 K and a background pressure of 1×10^{-6} mbar CO, SFG detects a single intense peak at 2100 cm^{-1}. After an exposure of 30 L CO at 100 K TPD indicated a single desorption peak at 140 K (Fig. 1b). The good resemblance of the spectrum in Fig. 1a with those of CO adsorption studies on Cu(100) indicates that CO is adsorbed on-top of Cu atoms. Taking into account that the CO saturation coverage on Cu(100) is 0.56 ML [42] and that the $Cu_3Au(100)$ surface is terminated by Cu(50%)–Au(50%) [38,39],[1] the total CO coverage on $Cu_3Au(100)$ is ~0.3 ML, which was also confirmed by TPD [43]. CO adsorption on Au atoms can be excluded at the low pressure and temperature used. One should note that the non-resonant SFG background signal is low (only ~5% of the maximum resonant signal) and has a phase that leads to nearly symmetric SFG peaks. The small linewidth (FWHM) of the SFG signal (7.5 cm^{-1}) indicates a well-ordered CO overlayer. Upon increasing the pressure to 1×10^{-5} mbar the SFG signal shifted to 2095 cm^{-1} and broadened. This is probably due to a loss of CO order at higher pressure as the packing density of CO on the surface is increased. The on-top CO band disappeared at 200 K, as expected from TPD.

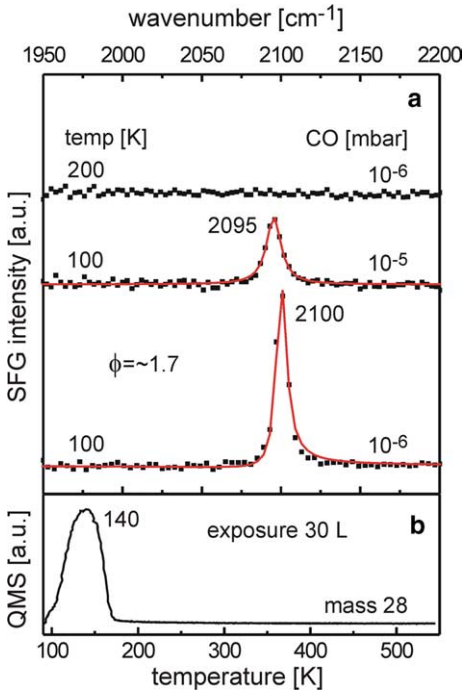

Fig. 1. (a) SFG and (b) TPD (mass 28) spectra of CO on $Cu_3Au(100)$. SFG spectra were measured at 100 K and 200 K with the indicated CO background pressure. For TPD, the surface was exposed to 30 L CO at 90 K (heating rate 1 K/s). Squares represent the experimental SFG data points, the solid lines are the result of fitting to a theoretical function (as described in [35]).

3.2. Adsorption of CO on $Nb_2O_5/Cu_3Au(100)$

After preparing a thin Nb_2O_5 film on $Cu_3Au(100)$, following the procedure described in [37] and Section 2, the oxide film was examined by LEED and AES. The LEED pattern (Fig. 2c) agrees well with the previous work and we refer to Starr et al. [37] for its description. The AES spectrum of the Nb_2O_5 film (not shown) indicated a Nb:O peak to peak ratio of ~1:1, suggesting a Nb:O ratio of 1:2.5,[2] consistent with the Nb_2O_5 stoichiometry.

With respect to CO adsorption, SFG and TPD spectra were recorded (Fig. 2a and b). At 1×10^{-6} mbar CO and 100 K, SFG detected resonant signals at 2118 cm^{-1} and 2165 cm^{-1} with an amplitude ratio of 5:1, respectively. Apparently, the CO signal on Nb_2O_5 is weaker than on Cu_3Au and based on a comparison of the CO SFG amplitudes in Figs. 1a and 2a, an overall CO coverage of ~0.15 ML is estimated for CO/Nb_2O_5. Due to the smaller resonant SFG signal the influence of the non-resonant background is more pronounced eventually leading to more asymmetric lineshapes (see Morkel et al. [35] for a full description). Comparing the CO-TPD areas of Figs. 1b and 2b indicates a CO coverage of ~0.1 ML, which is in reasonable agreement with the SFG value (due to the 30 L exposure the different sticking probabilities on the two surfaces seem to have only a minor influence). CO is most likely adsorbed on the Nb^{5+} cations of Nb_2O_5 [10].

The two CO-SFG peaks are consistent with two TPD desorption peaks at 112 K and 273 K, with a TPD peak area ratio of 2:1, respectively. The peak at 2165 cm^{-1} disappeared at ~150 K while that at 2118 cm^{-1} only vanished after annealing above 250 K. Consequently, the 112 K

[1] Normal to the (100) surface, $Cu_3Au(100)$ consists of alternating pure Cu(100) and 50%:50% Cu:Au layers [38,39].

[2] Taking into account the relative sensitivity factors (Nb: 1; O: 2.5) and the corresponding escape depths (Nb: ~0.7 nm; O: ~1 nm).

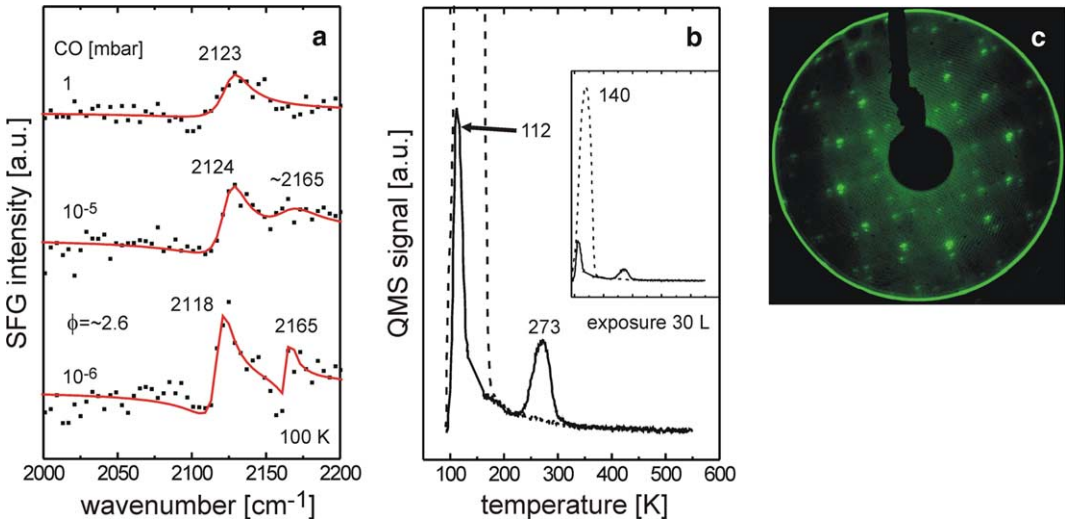

Fig. 2. (a) SFG and (b) TPD (mass 28) spectra of CO on a Nb_2O_5 thin film grown on $Cu_3Au(100)$. The dashed line in (b) shows the TPD trace of CO/Cu_3Au (Fig. 1b) for comparison. The LEED pattern of a Nb_2O_5 film is shown in (c).

desorption state can be assigned to the 2165 cm^{-1} SFG peak, while the 273 K desorption feature must be rather related to the 2118 cm^{-1} resonance. This is further supported by the resonance frequencies (higher ν_{CO} values typically indicate weaker bonding).

The high C–O stretching frequency of both species, compared to the CO gas phase value of 2143 cm^{-1} or to typical values of CO adsorbed on Pd (see below), indicates weak bonding of CO to Nb_2O_5. Taking into account resonance frequencies of CO on other oxides (for instance 2144 cm^{-1} for CO on well-ordered Ni^{2+} sites of NiO(111) [32]), the 2165 cm^{-1}/112 K species most likely originates from CO weakly bonded to Nb_2O_5 terraces (regular sites). The 2118 cm^{-1} species is tentatively assigned to CO bonded to (line- or point-)defects of the Nb_2O_5 film (see [37] for STM images), which seems plausible in light of the high desorption temperature of 273 K. The increased linewidth (13 cm^{-1}) of this species points to a less-ordered CO structure and may in fact contain some lateral interaction between CO molecules on the two different adsorption sites. In any case, based on this result we are certainly able to differentiate CO adsorption on Nb_2O_5 from that on Pd.

Upon increasing the pressure to 1×10^{-5} and 1 mbar, the SFG signals slightly shifted and broadened, similar to the observation made for CO/Cu_3Au. The (slightly) higher packing density at elevated pressure may again lead to a loss of order of the CO molecules, explaining the broadening.

3.3. Adsorption of CO on Pd–Nb_2O_5/$Cu_3Au(100)$

Pd particles were grown on the Nb_2O_5 film at 90 K. SFG spectra of adsorbed CO are collected in Fig. 3. Based on

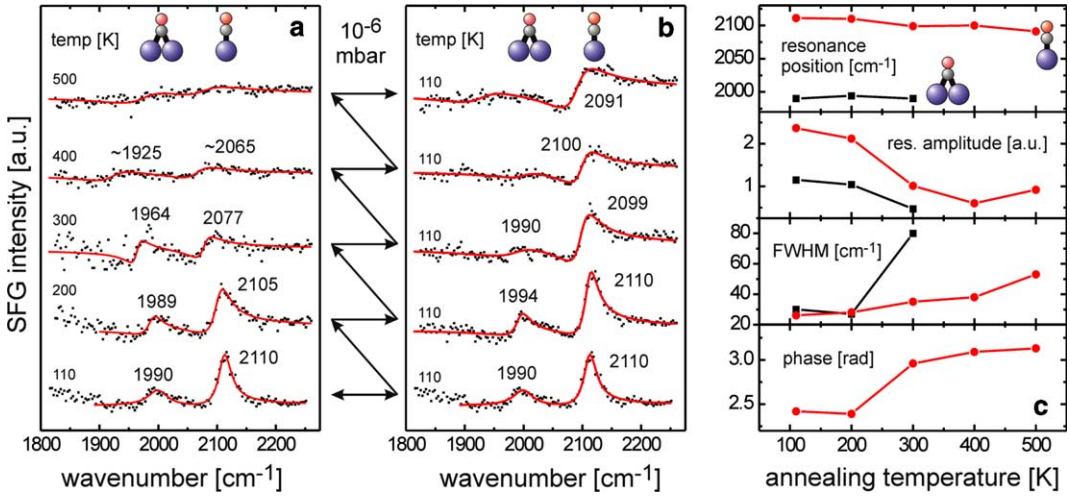

Fig. 3. (a) SFG spectra of CO (10^{-6} mbar) adsorbed on 3.5 nm Pd particles supported on Nb_2O_5/$Cu_3Au(100)$ at different temperatures. (b) SFG spectra of CO adsorbed on Pd particles measured after cooling the annealed surfaces of (a) in 10^{-6} mbar CO to 110 K. Values obtained for peak position, resonant amplitude, peak width (FWHM) and phase ϕ of the spectra in (b) are displayed in (c), both for on-top and bridge-bonded CO.

previous studies of CO-Pd/Al_2O_3/NiAl(1 1 0) [29,30,33–36], considering the CO SFG peak intensities and, in particular, the ratio between bridge and on-top bonded CO (see below), the Pd nanoparticles supported by Nb_2O_5 are about 3.5 ± 1 nm in size. Since the particle growth occurred at 90 K rough Pd particles are expected which is indeed consistent with the observed vibrational spectra. Experiments under UHV conditions as well as at mbar pressure are discussed in the following.

3.3.1. SFG and TPD studies under low pressure

Fig. 3 shows SFG spectra of 1×10^{-6} mbar CO on Pd–Nb_2O_5/Cu_3Au(1 0 0). The spectrum at 110 K can be considered a CO saturation spectrum. Two peaks were observed at 2110 cm^{-1} and 1990 cm^{-1}, typical of on-top and bridge-bonded CO on Pd nanoparticles, respectively. The assignment of the peak frequencies has been previously confirmed both by experimental [30,34] and theoretical work [44]. The spectrum at 10^{-6} mbar/110 K is comparable to that observed on 3.5 nm (rough) Pd particles on Al_2O_3, although the slightly higher on-top intensity on Pd–Nb_2O_5 may indicate a higher fraction of low-coordinated sites [29,34–36]. Here, CO adsorbed on Nb_2O_5 yielded only very small signals, if present at all (CO may rather diffuse from the oxide to the more stable Pd sites).

Taking the SFG spectrum of Fig. 1a again as reference, a total CO coverage of ~0.5 ML CO (per sample area) can be deduced. This is again backed up by the analysis of the CO-TPD traces in Figs. 1b and 4 (trace a), which yields the same value. As mentioned, comparing the SFG intensities and the on-top/bridge ratio (~2) to corresponding values for the CO-Pd/Al_2O_3/NiAl(1 1 0) system suggests a mean particle size of about 3.5 ± 1 nm (and an island density of $\sim 4 \times 10^{12}$ cm^{-2}). For hemispherical 3.5 nm particles at least 40% of the Nb_2O_5 surface is covered with Pd particles. Although a direct STM evaluation of the exact growth properties of Pd on Nb_2O_5 has not been performed yet, this estimation of Pd particle size is sufficient for the present study.

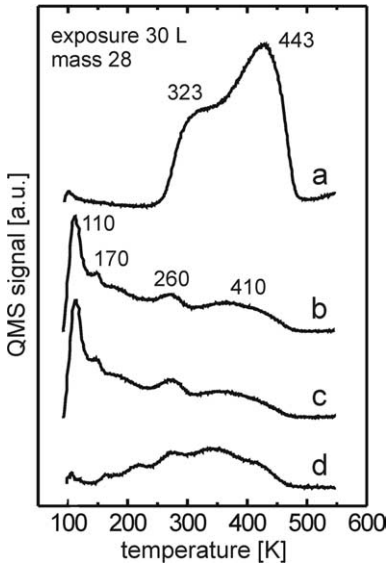

Fig. 4. Consecutive TPD spectra of CO on 3.5 nm Pd particles supported on Nb_2O_5 (exposure 30 L CO at 100 K): (a) TPD spectrum obtained from pristine Pd–Nb_2O_5/Cu_3Au(1 0 0), (b) second (repeated) TPD spectrum and (c) third (repeated) TPD spectrum. The CO-TPD spectrum (d) was acquired after exposing the annealed surface (after the third TPD) to 500 L of H_2 at 500 K, followed by cooling to 100 K in 1×10^{-7} mbar H_2.

Fig. 3a also shows SFG spectra of 1×10^{-6} mbar CO on Pd–Nb_2O_5 acquired at increasing temperature up to 500 K. A CO-TPD spectrum (exposure 30 L at 100 K) is displayed in Fig. 4 (trace a). Both SFG and TPD indicate the onset of CO desorption around 250 K with, according to SFG, on-top CO desorbing first. The on-top CO peak disappeared above 300 K while the bridged peak shifted to 1964 cm^{-1} at 300 K and disappeared above 400 K. Accordingly, the high temperature desorption in Fig. 4 (trace a) is mainly due to bridge-bonded CO. Hollow bonded CO cannot be fully ruled out but its contribution on rough Pd particles is typically very small [29,30,35,36].

During these annealing experiments, irreversible structural changes of the Pd–Nb_2O_5/Cu_3Au(1 0 0) model catalysts occurred that can also be characterized by SFG and TPD. After every annealing step in Fig. 3a, the catalyst was cooled down to 110 K in the CO atmosphere and another SFG spectrum was measured and compared to the initial spectrum at 110 K (Fig. 3b). After annealing to 200 K no significant changes were observed while annealing above 300 K resulted in pronounced alterations (Fig. 3b). The bridge-bonded CO peak nearly disappeared while on-top CO lost 58% of its initial amplitude and slightly broadened. The loss of strong CO binding sites is also evident from TPD (Fig. 4, trace b), indicating a 50% reduction in the overall CO adsorption capacity (details of the TPD spectra will discussed below). The shift in the on-top CO band from 2110 to 2099 cm^{-1} also points to a modification of the Pd surface. After annealing to 500 K the CO band shifted to 2091 cm^{-1} with a "remaining" CO coverage of ~0.2 ML at 110 K.

Fig. 3c collects the peak positions, resonant amplitude, linewidth (FWHM) and phase ϕ after the various annealing steps (peaks that were too weak for reasonable fitting were not included). Most importantly, there is a clear change in the phase ϕ between the resonant signals and the non-resonant background upon annealing to 300 K. This change in the surface susceptibility indicates that there is not only a simple restructuring or sintering of the Pd particles but that the overall electronic structure of the Pd–Nb_2O_5 system changes. One should note that the resulting phase was not observed for any material (Cu_3Au(1 0 0), Nb_2O_5/Cu_3Au(1 0 0), pristine Pd–Nb_2O_5/Cu_3Au(1 0 0)) discussed above. A possible explanation is that a "Pd–NbO_x mixed compound" is formed which is also supported by the TPD data.

Fig. 4 shows a series of TPD spectra of CO on Pd–Nb_2O_5/Cu_3Au(1 0 0) (exposure 30 L at 90 K). For the as-prepared sample (trace a) broad desorption signals appeared around 323 K and 443 K, indicating a CO coverage

of 0.5 ML (again using CO/Cu_3Au as reference). As discussed above, the low temperature desorption is (mostly) due to on-top CO (but may also obscure CO desorption from Nb_2O_5 at 273 K) while the high-temperature feature can be assigned to bridge-bonded CO [30,36]. For Pd–Al_2O_3 the different desorption states have been clearly differentiated by temperature-dependent IRAS [26,29].

After the first TPD of the pristine Pd–Nb_2O_5/Cu_3Au(100) system (up to 550 K), 30 L CO were again dosed and TPD was repeated. The consecutive TPD trace (b) was quite different from trace (a), while subsequent TPD profiles (c) did not show any further changes. In profile (b) the high temperature desorption states around 440 K had mostly disappeared, while new peaks were observed at 110 K, 170 K, 260 K and ~410 K. As mentioned, the overall amount of adsorbed CO was reduced to ~50% (i.e. the CO coverage in the annealed state was ~0.25 ML). The peaks at 110 K and 260 K are reminiscent of CO adsorbed on Nb_2O_5 (cf. Fig. 2b) while the broad peak at 350–410 K resembles CO desorption from Pd. At first, the TPD profile (b) seems to be a superposition of CO desorption from Nb_2O_5 and of a smaller contribution of CO desorption from Pd. Accordingly, one could suspect that the exposed Pd surface area was simply reduced upon annealing, e.g. by Pd sintering or by diffusion of Pd into the Nb_2O_5 film (or migration of Nb_2O_5 onto the Pd particles). However, the C–O stretching frequency after annealing (2090–2100 cm^{-1}) is different both from CO on large Pd particles [30,34–36] and from CO on a pristine Nb_2O_5 film (cf. Fig. 2a) and, taking into account the phase change described above, the formation of a new "Pd–NbO_x mixed compound" is most likely. A further observation that supports this suggestion is that the CO-TPD peak area in the annealed sample is about four times larger than that of CO on pristine Nb_2O_5, i.e. more CO adsorbs even on annealed Pd–Nb_2O_5 than on Nb_2O_5. Considering results from Carlson et al. [45,46] on Pd–Co particles, the decrease in the desorption temperature from 443 K to 370–410 K may be another indication for the formation of bimetallic-like mixed particles where Pd sites are modified by neighboring Nb atoms. Such a picture would be consistent with metal–support interaction as observed in heterogeneous catalysis [47–49].

We have also examined the effect of hydrogen reduction at 500 K on the annealed sample (Fig. 4, trace d).[3] However, the surface could not be further modified even by repeated H_2 treatments and the only effect was the absence of the 110/170 K CO desorption features, because these sites were blocked by adsorbed H (during TPD a small hydrogen desorption signal was observed at ~200 K).

With our experimental setup we have tried to examine the "Pd–NbO_x phase" by AES. However, in light of the small thickness of the thin film catalyst (0.4 nm Nb_2O_5 and ~1.5 nm Pd) the whole sample contributes to the AES spectrum, as also indicated by the observation of small Cu signals (AES spectrum not shown). Thus, a comparison of the Nb, O, and Pd AES signals did not allow following the compositional changes. Of course, an exact structure/composition characterization of the "Pd–NbO_x mixed compound" would be most interesting and may be subject of future STM, synchrotron XPS, etc. studies. One should finally note that annealing of Pd particles on Al_2O_3 up to 600 K did not induce significant changes with respect to CO adsorption, as monitored by SFG and TPD (annealing above 300 K rather resulted in an ordering of the particle surface [30]). The reducibility of Nb_2O_5 therefore seems to be an important parameter [4].

3.3.2. SFG spectroscopy under ambient pressure

SFG measurements on (freshly prepared) Pd–Nb_2O_5/Cu_3Au(100) were also extended to higher CO pressures up to 100 mbar. A temperature of 300 K, which is basically the onset temperature for the structural changes, was chosen for these experiments. As already shown in Fig. 3, annealing the sample in 1×10^{-6} mbar CO from 100 K to 300 K leads to a significant reduction of the on-top CO intensity (and to a beginning phase change). Consequently, the 10^{-6} mbar/300 K spectrum in Fig. 5 exhibits bridge (1979 cm^{-1}) and on-top (2095 cm^{-1}) CO peaks of similar amplitude.

When the CO pressure was increased up to 100 mbar, no significant changes were observed which indicates that saturation was already achieved at 10^{-6} mbar CO. In the 100 mbar spectrum a maximum was observed at 2140 cm^{-1} (not included in the fitting) which could be due to CO adsorbed on Nb_2O_5 but may also be induced

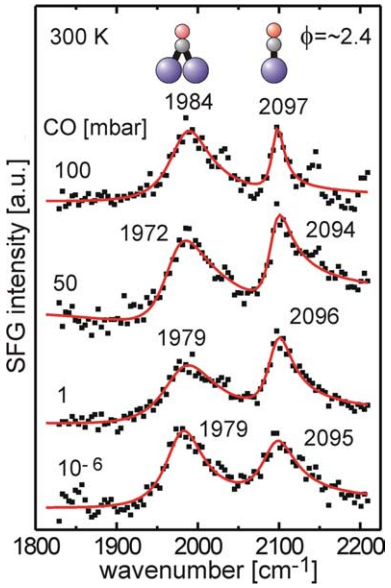

Fig. 5. SFG spectra of CO on 3.5 nm Pd particles supported on a Nb_2O_5 thin film grown on Cu_3Au(100). Spectra were taken at 300 K from 1×10^{-6} to 100 mbar CO.

[3] High temperature hydrogen reduction was reported to lead to Fischer–Tropsch catalysts highly selective for C^{5+} hydrocarbons [18].

by the CO gas phase. As described in [34,36] the SFG intensity must be normalized by the incident IR intensity. Since the IR intensity exhibits a maximum at 2143 cm^{-1} (due to the rovibrational CO gas phase spectrum), the SFG signal also does and the peak at 2143 cm^{-1} may therefore originate from the normalization (which may not be exact around this region of extreme IR intensity variation).

We have also performed experiments under catalytic reaction conditions and CO hydrogenation on Pd–$Nb_2O_5/Cu_3Au(100)$ was studied by gas chromatography at atmospheric pressure. The catalysts were exposed to 100 mbar CO and 400 mbar H_2 (using Ar as fill up gas to 1 bar) at temperatures up to 500 K. However, no product formation (such as methane or longer chain hydrocarbons) was observed even after 5–6 h reaction. Above 300 K no adsorbed CO was detected by SFG, indicating that the surface modification did also occur in the presence of high hydrogen pressure. The absence of products does, however, not necessarily indicate that the catalysts are inactive. The reaction rates may be simply too small to yield sufficient amounts of products on the small surface area of a model catalyst ($\sim$1 cm^2) that is measurable by GC. "Mixed metal–NbO_x compounds" have fact been proposed as key components of active catalysts [4,9,16,18,21]. Further studies are certainly required to better understand the interaction of metal nanoparticles with Nb_2O_5 thin film supports.

4. Conclusions

The adsorption of CO on Pd nanoparticles supported by $Nb_2O_5/Cu_3Au(100)$ was investigated by combined SFG and TPD studies from 100 K to 500 K and from UHV to 100 mbar. Annealing Pd–$Nb_2O_5/Cu_3Au(100)$ higher than 300 K lead to irreversible structural changes, indicated by a $\sim$50% loss of the CO adsorption capacity and pronounced changes of the adsorption states. Changes in the vibrational frequencies and phase in CO-SFG spectra suggest alterations in the electronic structure of the model catalyst by metal–support interaction, i.e. formation of "mixed Pd–NbO_x compounds", while simple structural changes or sintering of the Pd particles can be excluded. Furthermore, the new surface composition is different from pure Nb_2O_5, i.e. migration of Nb_2O_5 over Pd particles cannot explain the current findings. These effects were observed both under UHV and ambient pressure and may contribute to the catalytic properties of Nb_2O_5 supported metal nanoparticles.

Acknowledgements

AB gratefully acknowledges the Alexander von Humboldt Foundation for granting a fellowship. This work was partly supported by Priority Program SPP 1091 (Ru 831/1–4) of the German Science Foundation (DFG). We also thank F. Mendes and S. Shaikhutdinov for helpful discussions concerning the preparation of thin niobia films.

References

[1] I.E. Wachs, L.E. Briand, J.-M. Jehng, L. Burcham, X. Gao, Catal. Today 57 (2000) 323.
[2] K. Tanabe, Catal. Today 78 (2003) 65.
[3] T. Ushikubo, Catal. Today 57 (2000) 331.
[4] T. Uchijima, Catal. Today 28 (1996) 105.
[5] J.C. Védrine, G. Goudurier, A. Ouqour, P.G.P. de Oliveira, J.C. Volta, Catal. Today 28 (1996) 3.
[6] I.E. Wachs, Catal. Today 100 (2005) 79.
[7] I.E. Wachs, J.-M. Jehng, G. Deo, H. Hu, N. Arora, Catal. Today 28 (1996) 199.
[8] F.B. Noronha, A. Frydman, D.A.G. Aranda, C. Perez, R.R. Soares, B. Moraweck, D. Castner, C.T. Campbell, R. Frety, M. Schmal, Catal. Today 28 (1996) 147.
[9] Z. Hu, K. Kunimori, T. Uchijima, Appl. Catal. 69 (1991) 253.
[10] O.S. Aleksev, T. Beutel, E.A. Paukshtis, A. Ryndin, V.A. Likholobov, H. Knözinger, J. Mol. Catal. 92 (1994) 217.
[11] E. Iglesia, S.L. Soled, R.A. Fiato, G.H. Via, J. Catal. 143 (1993) 345.
[12] E. Iglesia, Appl. Catal. A 121 (1997) 59.
[13] T. Mori, A. Miyamoto, N. Takahashi, M. Fukagaya, T. Hattori, Y. Murakami, J. Phys. Chem. 90 (1986) 197.
[14] J.-M. Jehng, A.M. Turek, I.E. Wachs, Appl. Catal. A 83 (1992) 179.
[15] T. Iizuka, Y. Tanaka, K. Tanabe, J. Mol. Catal. 17 (1982) 381.
[16] E.I. Ko, M. Hupp, N.J. Wagner, J. Catal. 86 (1984) 315.
[17] R.R.C.M. Silva, J.M. Dalmon, R. Frety, M. Schmal, J. Chem. Soc. Faraday Trans. 89 (1993) 3975.
[18] F.M.T. Mendes, C.A.C. Perez, F.B. Noronha, M. Schmal, Catal. Today 101 (2005) 45.
[19] R. Brayner, D. dos Santos Lunha, F. Bozon-Verduraz, Catal. Today 78 (2003) 419.
[20] F.B. Noronha, M. Schmal, B. Moraweck, P. Delichere, M. Brun, F. Villain, R. Frety, J. Phys. Chem. B 104 (2000) 5478.
[21] F.B. Noronha, D.A.G. Aranda, A.P. Ordine, M. Schmal, Catal. Today 57 (2000) 275.
[22] M. Cherian, M.S. Rao, G. Deo, Catal. Today 78 (2003) 397.
[23] T. Ushikubo, Catal. Today 78 (2003) 79.
[24] H.-J. Freund, Angew. Chem. Int. Ed. Engl. 36 (1997) 452.
[25] C.T. Campbell, Surf. Sci. Rep. 27 (1997) 1.
[26] M. Bäumer, H.-J. Freund, Prog. Surf. Sci. 61 (1999) 127.
[27] M. Frank, M. Bäumer, Phys. Chem. Chem. Phys. 2 (2000) 3723.
[28] Sh. Shaikhutdinov, M. Heemeier, M. Bäumer, T. Lear, D. Lennon, R.J. Oldman, S.D. Jackson, H.-J. Freund, J. Catal. 200 (2001) 330.
[29] K. Wolter, O. Seiferth, H. Kuhlenbeck, M. Bäumer, H.-J. Freund, Surf. Sci. 399 (1998) 190.
[30] (a) H. Unterhalt, G. Rupprechter, H.-J. Freund, J. Phys. Chem. B 106 (2002) 356;
(b) G. Rupprechter, Ann. Rep. Prog. Chem. (C) 100 (2004) 237.
[31] G.A. Somorjai, G. Rupprechter, J. Phys. Chem. B 103 (1999) 1623.
[32] A. Bandara, S. Dobashi, J. Kubota, K. Onda, A. Wada, K. Domen, C. Hirose, S.S. Kano, Surf. Sci. 387 (1997) 312.
[33] T. Dellwig, G. Rupprechter, H. Unterhalt, H.-J. Freund, Phys. Rev. Lett. 85 (2000) 776.
[34] G. Rupprechter, H. Unterhalt, M. Morkel, P. Galletto, L. Hu, H.-J. Freund, Surf. Sci. 502–503 (2002) 109.
[35] M. Morkel, H. Unterhalt, T. Klüner, G. Rupprechter, H.-J. Freund, Surf. Sci. 586 (2005) 146.
[36] M. Morkel, G. Rupprechter, H.-J. Freund, Surf. Sci. Lett. 588 (2005) L209.
[37] (a) D.E. Starr, F.M.T. Mendes, J. Middeke, R.P. Blum, H. Niehus, D. Lahav, S. Guimond, A. Uhl, T. Klüner, M. Schmal, H. Kuhlenbeck, S. Shaikhutdinov, H.-J. Freund, Surf. Sci. 599 (2005) 14;

(b) J. Middeke, R.-P. Blum, M. Hafemeister, H. Niehus, Surf. Sci. 587 (2005) 219.
[38] H. Niehus, C. Achete, Surf. Sci. 289 (1993) 19.
[39] H. Niehus, R. Blum, D. Ahlbehrendt, Surf. Rev. Lett. 10 (2003) 353.
[40] (a) Y.R. Shen, Nature 337 (1989) 519;
(b) Y.R. Shen, Surf. Sci. 299–300 (1994) 551.
[41] (a) A. Tadjeddine, A. Peremans, Surf. Sci. 368 (1996) 377;
(b) M. Buck, M. Himmelhaus, J. Vac. Sci. Technol. A 19 (2001) 2717;
(c) H. Härle, A. Lehnert, U. Metka, H.R. Volpp, L. Willms, J. Wolfrum, Chem. Phys. Lett. 293 (1998) 26;
(d) B. Bourguignon, S. Carrez, B. Dragnea, H. Dubost, Surf. Sci. 418 (1998) 171;
(e) V.L. Zhang, H. Arnolds, D.A. King, Surf. Sci. 587 (2005) 102.
[42] J.C. Tracy, J. Chem. Phys. 56 (1972) 2748.
[43] G.W. Graham, Surf. Sci. 187 (1987) 490.
[44] I.V. Yudanov, R. Sahnoun, K.M. Neyman, N. Rösch, J. Hoffmann, S. Schauermann, V. Johánek, H. Unterhalt, G. Rupprechter, J. Libuda, H.-J. Freund, J. Phys. Chem. B 107 (2003) 255.
[45] A.F. Carlsson, M. Bäumer, T. Risse, H.-J. Freund, J. Chem. Phys. 119 (2003) 10885.
[46] A.F. Carlsson, M. Naschitzki, M. Bäumer, J. Phys. Chem. B 107 (2003) 778.
[47] K. Hayek, M. Fuchs, B. Klötzer, W. Reichl, G. Rupprechter, Top. Catal. 13 (2000) 55.
[48] S. Penner, D. Wang, D.S. Su, G. Rupprechter, R. Podloucky, R. Schlögl, K. Hayek, Surf. Sci. 532–535 (2003) 276.
[49] S. Bernal, J.J. Calvino, M.A. Cauqui, J.M. Gatica, C. Larese, J.A. Perez-Omil, J.M. Pintado, Catal. Today 50 (1999) 175.